Charge Separation in the Aerodynamic Breakup of Micrometer-Sized Water Droplets

Lloyd W. Zilch, Joshua T. Maze, John W. Smith, George E. Ewing,* and Martin F. Jarrold*

Chemistry Department, Indiana University, 800 East Kirkwood Avenue, Bloomington, Indiana 47405

Charged water droplets generated by electrospray, sonic spray, and a vibrating orifice aerosol generator (VOAG) have been studied by digital macrophotography and image charge detection mass spectrometry. Image charge detection mass spectrometry provides information on the droplet size, charge, and velocity after transmission through a capillary interface. The digital images provide the droplet size distribution before they enter the capillary. Droplets with $10-100$ μm radii generated by sonic spray and VOAG are reduced to $2-3$ μm radii by transmission through the capillary interface. The droplets from sonic spray and VOAG are much more highly charged than expected for random charging, and positive droplets are much more prevalent than negative. For positive mode electrospray, >99% of the detected droplets carry a positive charge, whereas for negative mode electrospray, <30% of the detected droplets carry a negative charge (i.e., >70% carry a positive charge). These observation can all be accounted for by the aerodynamic breakup of the droplets in the capillary interface. This breakup reduces the droplets to a terminal size at which point further breakup does not occur. Charge separation during droplet breakup is responsible for the relatively high charges on the sonic spray and VOAG droplets and for the preference for positively charged droplets. The charge separation can be explained using the bag mechanism for droplet breakup and the electrical bilayer at the surface of water.

Introduction

Charge separation in water droplets plays a role in many natural phenomena. The electrification of thunderstorms is perhaps the most obvious example. This process was studied even before Franklin's famous experiment of "drawing down the lightning to ascertain its sameness with the electric field". However, despite more than two and a half centuries of investigation, the processes that generate the charge separation in thunderstorms are still not completely understood.[1–10]

Another natural phenomenon that results from charge separation is waterfall electrification. It has been known for many years that the water at the base of a waterfall is positively charged, whereas the surrounding air acquires a negative charge. Lenard,[11] who studied waterfalls in the Alps and performed laboratory experiments on this phenomena, reported in 1892 that the charge separation results from the disruption of the water surface by splashing and bubbling. The splashing and bubbling leads to the formation of small negatively charged droplets.

A similar effect has been observed in the aerodynamic breakup of water droplets.[12,13] In 1909, Simpson showed that the breakup of uncharged distilled water droplets by a strong vertical air jet led to the formation of large fragments that carried a positive charge, whereas the surrounding air acquired a negative charge.

Charged droplets are important in many technological applications, for example, ink-jet printing and electrospray processes. Electrospray ionization[14,15] has been responsible for a revolution in the application of mass spectrometry based methods to the analysis of biological molecules. The mechanism by which desolvated ions are generated by electrospray has been a topic of heated discussion. The current consensus[16–20] is that the small charged droplets generated by electrospray evaporate and shrink until they reach a point where the electrostatic forces exceed surface tension (the Rayleigh limit[21]). The droplets then discharge by emitting a jet of small highly charged droplets. This evaporative shrinking and jetting process is thought to continue until the droplets become small enough that unsolvated ions can be generated from them.[22–24]

In this manuscript we report studies of charged water droplets generated by electrospray, sonic spray,[25,26] and a vibrating orifice aerosol generator (VOAG). The droplets are transmitted through a capillary interface and then image charge detection mass spectrometry is used to examine their charge, velocity, and size. Digital macrophotography is used to determine the size of the droplets before they enter the capillary interface. We have previously reported the charge, velocity, and size distributions[27,28] for droplets detected from positive mode electrospray. A surprising feature of these results is the observation of a small number of negatively charged droplets. We suggested that the oppositely charged droplets might result from a bipolar fission process where the electrostatic barrier for fission of a charged droplet is lowered by incorporating a small oppositely charged droplet between the larger progeny.

The idea of forming a negatively charged satellite droplet from the fission of a much larger positively charged droplet was first considered by Sanford in 1918.[29] He noted that the breakup of millimeter-sized droplets is usually accompanied by the formation of a small satellite droplet between the two main progeny droplets. If the breakup is slightly asymmetric and the satellite droplet remains attached to the smaller progeny droplet for longer than to the larger, then the satellite droplet will be negatively charged by induction.

Although bipolar fission may account for the observation of a small fraction (<1%) of negatively charged droplets from positive mode electrospray, we report here that the droplets detected from negative mode electrospray after transmission through the capillary interface are predominantly (>70%) positively charged. It is difficult to see how an excess of oppositely charged droplets could be accounted for by bipolar

* Corresponding authors. E-mail: ewingg@indiana.edu (G.E.E.), mfj@indiana.edu (M.F.J.).
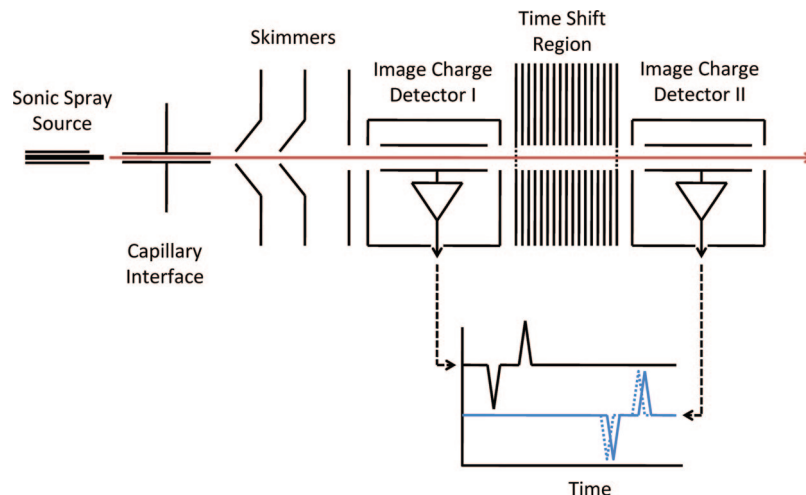
Charge Separation in the Breakup of Water Droplets

J. Phys. Chem. A, Vol. 112, No. 51, 2008 **13353**

Figure 1. Schematic diagram of the experimental apparatus. The apparatus is shown equipped with a sonic spray source. Measurements were also performed with an electrospray source and a vibrating orifice aerosol generator (VOAG). The plot at the bottom of the figure shows a cartoon of the signal obtained from the first and second image charge detectors. The dashed blue line shows the signal without a voltage on the time shift region, and the solid blue line shows the signal with a voltage that slows down the arrival of the droplet. The time shift provides the *m/z* ratio.

fission. We find that the strong preference for positively charged droplets extends to droplets generated by sonic spray and by VOAG. In these later cases, the average charge is also orders of magnitude larger than expected for random charging. We suggest that all these observations can be accounted for by the charge separation that occurs in the aerodynamic breakup of the droplets in the capillary interface.

Experimental Methods

Droplet Generation: Electrospray, Sonic Spray, and VOAG. Droplets are generated by electrospray, sonic spray, or by a VOAG.

A polyimide-coated fused-silica capillary with an inner diameter of 250 μm (Polymicro Technologies, Phoenix, AZ) was used for the electrospray source. Electrical contact to the water was made through a tee union and a stainless steel electrode held at +4.5 or −4.5 kV. The capillary was fed with water at 1 mL/h by a syringe pump. We used degassed, purified (18.2 MΩ), and filtered (20 nm) water or degassed, HPLC grade water (Omni-Solv, EMD Chemicals Inc.). Water from both sources gave similar results.

The sonic spray source was modeled after the design of Takats et al.[30] The inner fused-silica capillary has an i.d. of 100 μm and an o.d. of 200 μm. The outer capillary had an i.d. of 250 μm and an o.d. of 350 μm. (Both capillaries were obtained from Polymicro Technologies, Phoenix, AZ.) The inner capillary was fed with water at 2−4 mL/h by a syringe pump. The outer capillary was fed with ultrahigh purity nitrogen (Airgas) at 400−800 kPa.

The VOAG was constructed from a piezoelectric tube (PT 120.00 obtained from Physik Instrumente, Auburn, MA) and glass microtips (World Precision Instruments, Sarasota, FL) held in place by a stainless steel holder. The piezoelectric tube was driven at 42 kHz with a peak-to-peak voltage of 250−300 V by an Agilent 33220A function generator and a custom-built amplifier. The water was gravity fed and connected to the glass tip by Teflon tubing.

Droplet Charge and Velocity Measurements. A schematic diagram of the image charge detection mass spectrometer used in these studies is shown in Figure 1.[27,28] The droplets enter the vacuum system through a grounded 500 μm internal diameter, 12.7 cm long stainless steel capillary. After passing through

the capillary, they travel through three differentially pumped chambers separated by grounded conical skimmers. The pressures in these chambers are $\sim$0.35, $\sim$5 × 10^{-5}, and $\sim$2 × 10^{-6} Torr during operation. The final chamber contains two image charge detectors separated by a time shift region (see below). The charge detectors were modeled after the design of Fuerstenau and Benner.[31] The detectors consist of a central stainless steel tube (0.65 cm internal diameter and 3.81 cm long) centered inside a grounded stainless steel shield and connected to a charge-sensitive preamplifier (Amptek A250) through an external JFET (2SK152). When a charged droplet enters the tube, an equal but opposite charge is impressed on the tube. The output from the charge-sensitive preamplifier is amplified and differentiated by an Ortec 572A amplifier, recorded with a 14-bit transient digitizer (AlazarTech, ATS460), and then transferred to a computer.

The signal recorded by the transient digitizer consists of a peak when the droplet enters the charge detector and a peak of the opposite polarity when the droplet leaves, as shown in the plot at the bottom of Figure 1. The area of the peak is proportional to the charge. The time between the entrance and exit peaks along with the effective length of the image charge detector (see below) provides a measure of the velocity.

The electrospray current was monitored during some of the experiments using a home-built current-to-voltage converter with a rise time of less than 1 μs. The current-to-voltage converter is connected to the capillary interface and the cylindrical metal plug that holds it in place. The capillary and its holder are electrically isolated from the rest of the apparatus. This approach to measuring the electrospray current avoids operating the current-to-voltage converter at the electrospray voltage. The average electrospray current on the capillary and its holder was the same as that measured with a DVM directly at the electrospray needle. The output from the current-to-voltage converter is monitored with a digital oscilloscope and can be simultaneously recorded with the droplet signals in the second channel of the transient digitizer.

Droplet Mass Measurements. The mass of a droplet can be determined from measurement of its charge and *m/z* ratio. The droplets are accelerated in the capillary interface to velocities of around 200−300 ms^{-1} (see below), and so to determine their *m/z* ratio it is necessary to accelerate or

decelerate them through a known potential and determine the effect on their velocity. In previous work, we employed a pulsed acceleration approach to measure the *m/z* ratio for individual electrosprayed water droplets.[28] Combining the measured *m/z* ratio with the charge measurement provides a mass for individual droplets. In the pulsed acceleration approach, the initial velocity of the droplet is measured with an image charge detector, the droplet is then pulse accelerated through a known potential, and its velocity is remeasured with a second image charge detector. The change in velocity provides a measure of the *m/z* ratio. However, when we tried to apply this method to droplets from sonic spray, we found that the shift in the velocity was too small to provide a reliable value for the *m/z* ratio. For this reason a different approach is taken here.

Instead of using a pulsed accelerator, we employ a region located between two image charge detectors where the droplets are accelerated and decelerated by a symmetric triangular-shaped potential ramp. The velocity of a given droplet should be the same in both detectors, but the arrival time in the second detector is shifted from the value expected from the average velocity and the known distance between the detectors. The mass-to-charge ratio can be deduced from the time shift and the potential on the ramp. The advantages of this approach are (1) we can use higher voltages than employed in the pulse accelerator, and hence, in principle, analyze higher mass-to-charge ratios, and (2) the potential gradients are gentler than used in the pulsed accelerator (the droplets may be discharged by high electric fields[32,33]).

The time shift region consists of a stack of 45 annular electrodes connected by resistors. The two end electrodes are connected to ground, and the center electrode is connected to a high-voltage power supply capable of providing ±20 kV. Fine woven stainless steel grids (0.002 wire diameter, 60 wires per inch) cover the apertures of the two end electrodes. However, to minimize the number of grids, we do not use a grid on the electrode at the center of the time shift region to define the apex of the triangular potential, and so the potential deviates slightly from a uniform triangular potential ramp near the apex (there is a saddle point at the center).

The experiment can be operated in two modes: (1) acceleration mode, where the charged droplets are initially accelerated in the time shift region and then decelerated back to the same potential (ground), and (2) deceleration mode, where the charged droplets are first decelerated and then accelerated. In the acceleration mode the droplet arrives at the second detector at a shorter time than predicted in the absence of the time shift voltage, and in the deceleration mode the droplet arrives at the second detector at a longer time than predicted (see Figure 1). Both modes can be used to determine the mass-to-charge ratio. In the deceleration mode the time shifts are larger than in the acceleration mode, and so the deceleration mode is more accurate. However, the deceleration mode has a cutoff that results when the energy of the macroion is insufficient to overcome the time shift voltage.

Droplet Imaging. Photographs were taken of the droplets produced by the sonic spray and VOAG using a Canon EOS 5D digital camera with a Canon MP-E65 f/2.8 macrolens and a Canon EF 2 × 11 extender. The sonic spray images were recorded at 5× and 10× magnification, with a shutter speed of 0.1 s, and flash illumination from a hemispherical array of 60 light-emitting diodes (LEDs): 20 red, 20 blue, and 20 green (Besthongkong.com, part nos. BURLC1363W10BA40, BU-BC1363W10BA13, and BUPGC1363W10BA40). The three LED groups are fired for 500 ns in sequence, with 10 *μ*s between
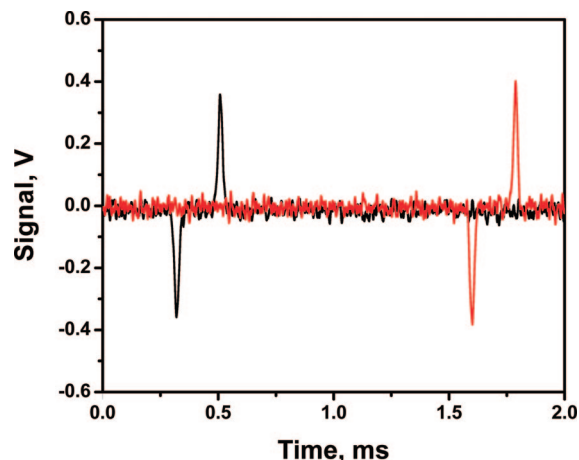

Figure 2. Example of the signals obtained from the first and second image charge detectors. The black line shows the signal from the first detector, and the red line shows the signal from the second. The first peak is negative in both traces indicating that the droplet is positively charged. The time between the negative and positive peaks in each trace provides a measure of the droplet velocity.

the pulses going to the different colored LED groups. Since the shutter remains open for the firing of all three groups of LEDs, three different colored images are overlaid in a single photograph. This approach allows us to investigate changes occurring on a 10 *μ*s time scale. The sonic spray source was detached from the rest of the image charge detection mass spectrometer to record the images because there is insufficient space to accommodate the camera and the hemispherical lighting array. However, images of the VOAG droplets were recorded in situ (i.e., with the VOAG attached to the image charge detection mass spectrometer). The VOAG photographs were taken at 5× magnification with a shutter speed of 0.1 s and with illumination from one white LED (Besthongkong.com, part no. BUWLC1363W10BA60) that was flashed with 25 V for 500 ns.

Results

Charge and Velocity Distributions. Figure 2 shows examples of the signals recorded in the first (black) and second (red) image charge detectors. The first (negative) peak results when the droplet enters the image charge detection cylinder, and the second (positive) peak results when it leaves. The first peak in both traces is negative, which indicates that the droplet is positively charged. The time between the negative and positive peaks in each trace provides the transit time through the detector which, with the effective length of the detector,[34] provides a measure of the droplet velocity. The area under the peaks is proportional to the charge on the droplet. The proportionality constant is determined by introducing a calibrated voltage pulse into a test capacitance attached to the image charge detection tube (see ref 28 for details). The time between the signals in the first and second detectors is used to deduce the *m/z* ratio of the droplet.

The output from the transient digitizer consists of thousands of files, each one containing a droplet signal. The data are analyzed off-line using a computer program which locates the droplet signals, determines the charge and velocity of the droplet, and tabulates the results. In order to be accepted, the transient must pass several tests: the baseline should be constant and not have any excess noise, the transient should contain the signal from only a single droplet, and the areas of the entrance and exit peak must agree within narrow limits.
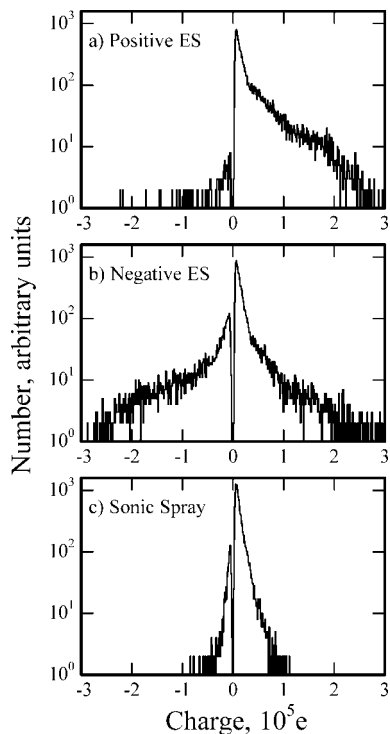
Charge Separation in the Breakup of Water Droplets

J. Phys. Chem. A, Vol. 112, No. 51, 2008 **13355**

Figure 3. Charge distributions obtained for droplets from (a) positive mode electrospray, (b) negative mode electrospray, and (c) sonic spray.

Histograms of the charge distributions obtained with the first image charge detector for three different experimental configurations are shown in Figure 3. Figure 3a shows the histogram obtained for the droplets detected from positive mode electrospray. Most of the detected droplets are positively charged, though a small fraction (0.7%) carries a negative charge. The charge distribution for the positive droplets peaks at low charge but has a tail which extends to almost 300 000 elementary charges (e). The results reported here for positive mode electrospray are similar to those previously reported by some of us.[27] We reproduce them here to compare with the results for negative mode electrospray, sonic spray, and VOAG. The results obtained by these later methods have not been presented elsewhere.

The intensity in the histogram in Figure 3a goes to zero at zero charge. This results from the sensitivity of the image charge detectors: if the charge on a droplet is too low, the signal is lost in the noise. In the measurements reported, the droplet signals become too small to detect for charges of 1000−2000 e.

Figure 3b shows the charge distribution for droplets detected from negative mode electrospray. The droplets from negative mode electrospray are expected to be negatively charged. Surprisingly, most of the detected droplets (77%) are positively charged. The charge distributions for both the positive and negative droplets peak at low charge and have long tails. The tail for the negative droplets is larger than for the positive, and the average charge for the negative droplets is larger than for the positive. The number of droplets detected per unit time for negative mode electrospray is much smaller than for positive mode.

Figure 3c shows the droplet charge distribution for droplets detected from sonic spray. The droplets are predominantly (91%) positively charged. The charge distributions peak at low charge and have tails which extend to around 100 000 e, which is significantly less than for the electrosprayed droplets. We do
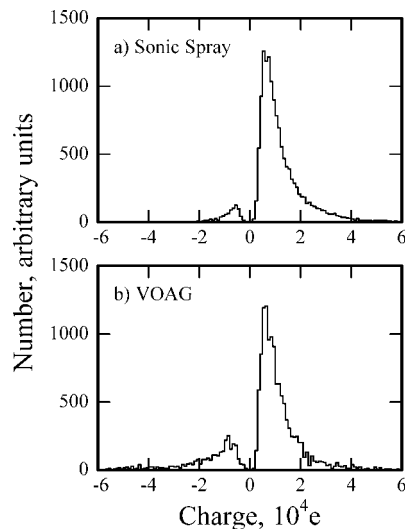

Figure 4. Charge distributions obtained for droplets from (a) sonic spray (an expanded view of results from Figure 3) and (b) VOAG (vibrating orifice aerosol generator).
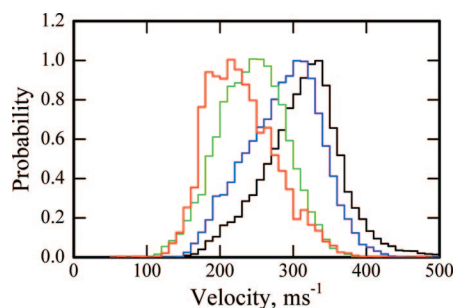

Figure 5. Velocity distributions obtained for droplets from positive mode electrospray (black), negative mode electrospray (blue), sonic spray (green), and VOAG (red).

not apply a voltage to the sonic spray source. However, because of the strong bias toward positively charged droplets we were concerned that the charge distribution might be influenced by stray electric fields. To address this concern we surrounded the sonic spray source by a grounded shield made from copper mesh. The charge distribution remained the same.

Figure 4 shows charge distributions obtained from (a) sonic spray (an expanded view of the results from Figure 3) and (b) VOAG. The charge distributions for the droplets detected from VOAG are almost identical to those detected from sonic spray, except that the number of negatively charged droplet is slightly larger.

Figure 5 shows velocity distributions obtained for all (i.e., positive and negative) droplets from positive mode electrospray (black line), negative mode electrospray (blue line), sonic spray (green line), and VOAG (red line). The velocity results from acceleration in the capillary interface that transports them from atmospheric pressure into the vacuum chamber. The distributions for the droplets from electrospray peak at around 320 ms^{-1}. The velocities for the droplets from sonic spray and VOAG peak at lower velocities, around 250 and 210 ms^{-1}, respectively.

Juraschek and Röllgen[35] have identified three electrospray modes that they labeled axial spray modes I, II, and III. Mode I consists of low-frequency (∼30 Hz) fluctuations in the electrospray current where the "on" section is made up of high-frequency oscillations (1−2 kHz) due to the Taylor cone pulsing and creating droplets. In the low-frequency "off" mode the Taylor cone is in a relaxed, nonspraying state. Mode II consists entirely of constant high-frequency (1−2 kHz) pulses in the

current. There are no low-frequency fluctuations in mode II. Mode III is a continuous spraying mode with no current pulsations with frequencies below 1 MHz.

To determine which of the three modes our source was operating in we monitored the electrospray current using the current-to-voltage converter attached to the capillary interface and its holder. We found that under our conditions the source fluctuated between axial modes I and II for both positive mode and negative mode electrospray. The transition between these modes could be induced, to at least some extent, by adjusting the liquid flow rate or by changing the distance between the electrospray needle and the capillary interface. The electrospray current and droplet signals were recorded simultaneously by the transient digitizer. From these results we found that the droplets generated were essentially the same in both of the two modes. The third mode, continuous spraying mode III, was observed for brief periods of time for positive electrospray, but we did not find conditions where the electrospray would stay in this mode for a significant fraction of the time.

The current measured on the capillary interface and its holder was positive for positive mode electrospray and negative for negative mode. As described above >99% of the droplets detected from positive mode electrospray are positively charged, whereas for negative mode electrospray >70% of the droplets are positive even though the electrospray current is negative. For sonic spray we could not detect a net current. This was confirmed by spraying into a large Faraday cup containing fine mesh to capture the charge. The absence of a net current is expected because the sonic spray source is electrically isolated; thus, the number of positive and negative charges leaving the source must balance. Recall that for sonic spray the detected droplets are predominantly positively charged, even though no net current is generated. This is analogous to the situation for negative mode electrospray, where most of the droplets detected are positive even though the electrospray current is negative.

Droplet Mass Measurements. To measure the *m/z* ratio we employ two image charge detectors separated by a region where the droplets are decelerated and accelerated by a symmetric voltage ramp with a shape that is close to triangular. The velocity of the droplet should be the same in both detectors, but the arrival time in the second detector should be shifted from that expected from the velocity and the known distance between the detectors.

To implement this approach we determine the velocities in both detectors and then from the average velocity we predict the transit time between the two detectors. We define the time shift as the transit time predicted from the average velocities minus the measured transit time. Histograms of the time shifts for positive droplets from sonic spray are shown in Figure 6. The red line shows the time shifts obtained with no voltage on the time shift region. In this case all the droplets should have zero time shift. The distribution of the time shifts found here reflects the uncertainty in the velocity determinations. The black line in Figure 6 shows the histogram recorded with +15 kV on the center electrode of the time shift region. With the voltage off, the distribution is centered around zero and has a standard deviation of 3.75 μs. With the voltage on, the distribution shifts by an average of −1.86 μs and has a standard deviation of 3.87 μs. The standard deviation of the shifted distribution contains contributions from the uncertainty in the velocity determination and from the variation in the time shifts. Assuming these two quantities are uncorrelated they can be separated to give the standard deviation due to the variation in time shifts alone,[36] which is 0.96 μs. The small time shift indicates a large mass-
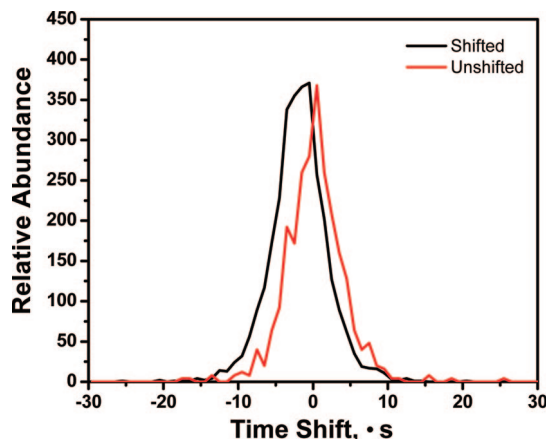

Figure 6. Plot of time shifts measured without a voltage on the acceleration region (red) and with +15 000 V on the center electrode of the time shift region (black).

to-charge ratio. Because the uncertainty from the velocity determination is larger than the average time shift we cannot analyze these results and obtain a distribution of the mass-to-charge ratios. However, we can obtain an estimate of the average mass-to-charge ratio from the average time shift.

In the time shift region, the times spent being accelerated and decelerated are the same, and the time shift due to an ideal triangular voltage ramp is

$$\Delta t = t_1 - t_2 = \frac{l}{u} - \frac{2(\sqrt{u^2 + al} - u)}{a} \qquad (1)$$

where t_1 is the predicted transit time through the acceleration region with no voltage applied and t_2 is the measured transit time with the voltage on. l is the length of the time shift region, u is the initial velocity, and a is the acceleration in the first leg of the time shift region (i.e., a is positive if the macroions are accelerated and then decelerated in the time shift region and negative if the macroions are decelerated first). a is given by

$$a = -\frac{z}{m} \frac{Ve}{l/2} \qquad (2)$$

where V is the voltage applied to the center electrode of the acceleration region. These equations can be rearranged to yield an expression for the mass-to-charge ratio

$$m/z = -\frac{(l/u - \Delta t)^2 eV}{2l\Delta t u m_u} \qquad (3)$$

where m_u is the atomic mass constant. From above, the average time shift is −1.86 μs and the average initial velocity is 260 ms⁻¹, from which the average m/z is 3.85×10^9 Da. The average charge is 12 600 e, and so the average mass of the droplets is 8.06×10^{-14} kg, which corresponds to an average radius of 2.7 μm. Droplets from the VOAG source yielded similar results; the average radius in this case was 3.0 μm.

Since the standard deviation in the time shifts (0.96 μs) (see above) is not small compared to the average time shift (−1.86 μs) there is a concern that using the average time shift in eq 3 will not provide the true average m/z. Under our conditions, $l/u \gg \Delta t$, and so m/z is proportional to Δt^{-1}. If the time shift distribution is Gaussian, with a standard deviation of 0.96 μs, then we estimate that the average m/z is underestimated by ~50%. Since the droplet radius is proportional to $(m/z)^{1/3}$, this translates into ~15% underestimate of the droplet radius.

Charge Separation in the Breakup of Water Droplets
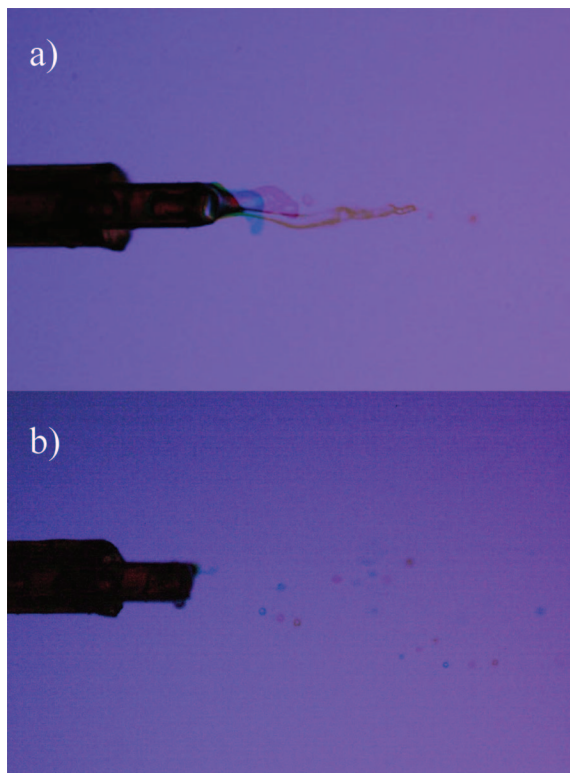
J. Phys. Chem. A, Vol. 112, No. 51, 2008 **13357**

Figure 7. Photographs of the operating sonic spray source. Each photograph is an overlay of three images recorded with 500 ns long blue, red, and green flashes spaced by 10 μs. The images obtained with the red flash appear purple, and the images from the green flash appear brown. The upper image shows a filament being pulled from the sonic spray source. The lower image shows droplets from the breakup of the filament. In several cases the droplets are moving in the focal plane, and a sequence of blue, purple, and brown images is apparent. The trajectory and velocity of the droplets can be determined from the images.

Finally, as noted above, the potential in the time shift region deviates from an ideal triangular potential ramp used above to analyze the results because the apex is not defined and there is a saddle point at the center. The deviation of the potential from the ideal triangular shape is 14% at the saddle point (according to SIMION 7.0[37]). Since the calculated mass is proportional to the maximum voltage on the center lens element, this gives a worst case error of 14% for the mass and 4.5% for the radius. In fact the error is much less. For the outer 92% of the ramp, the potential deviates by less than 5% from the ideal triangular form. The central region does have a significant dip, but this section has a small effect on the overall time shift.

Before entering the time shift region, the droplets pass through a 0.1 cm diameter collimating aperture which constrains them to the central portion of the time shift region (the time shift electrodes have an inner diameter of 2.4 cm). The variation in the maximum potential that the droplets experience across the 1.0 mm diameter defined by the entrance aperture is less than 0.25%. Hence the mass dispersion introduced by the variation in the maximum potential is less than 0.25%.

Imaging Droplets from Sonic Spray and VOAG. We took a large number of images of the operating sonic spray source which together provide a clear picture of how it functions. Figure 7 shows the source in two representative modes of its operation. As a point of reference, the outside diameters of the inner and outer capillaries of the source are 200 and 350 μm. The images were recorded by triggering arrays of different colored LEDs (blue, red, and green) at 10 μs intervals. In Figure 7, the image
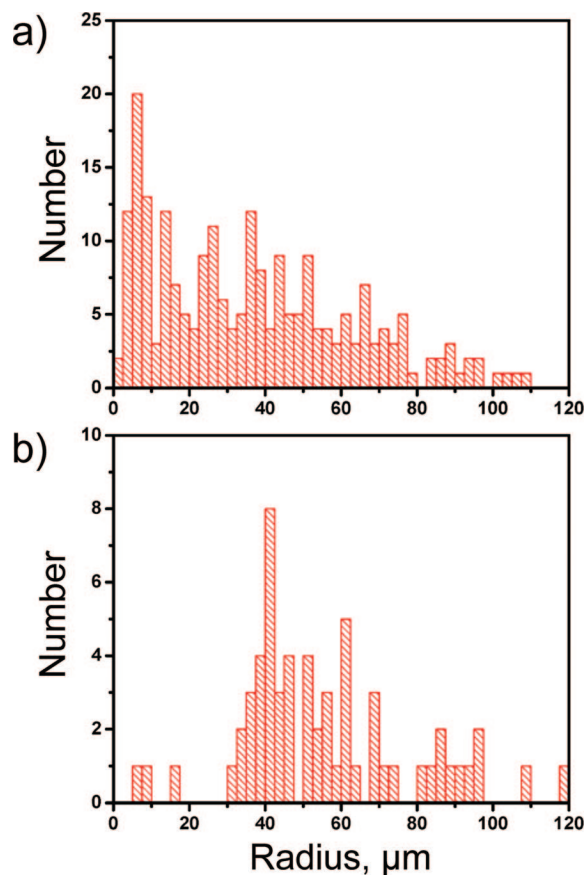

Figure 8. Histograms of the droplet radii determined from the photographs for (a) sonic spray and (b) VOAG.

recorded by flashing the red LEDs is purple, and the image obtained with the green LEDs appears brown.

The images in Figure 7a show a filament being pulled out of the inner capillary and beginning to break up into droplets. Figure 7b shows the droplets that result from the breakup of the filament.

In summary, the sequence of events is (1) a small droplet begins to form at the end of the inner capillary, (2) the droplet is suddenly pulled into a fine filament, and (3) the filament breaks up into droplets. When the filament is pulled, it draws out the water from near the end of the capillary. It takes a short time to replenish the water and form another small droplet at the end of the capillary, so the sonic spray source produces bursts of droplets. The cycle time depends on the liquid and gas flow rates.

Information about the size distribution of the droplets generated by sonic spray was obtained by analyzing the images. Only droplets that were in focus were included. The depth of field is small (around 100 μm at f/7 used here), and so only a narrow (though representative) slice of droplets are analyzed. The length scale was calibrated by photographing an electro-formed nickel mesh (0.5296 mm grid spacing and 0.03505 mm wire thickness from Precision Eforming LLC, Cortland, NY) that is located in the same plane as the droplets.

Figure 8a shows the radius distribution obtained for the sonic spray droplets. The distribution is broad; it peaks at around 6 μm and extends out to over 100 μm. The droplets detected here are much larger than detected in the mass measurements (where the average radius was 2.7 μm). A higher liquid flow rate and a lower gas flow rate produces larger droplets, and a lower liquid flow rate and higher gas flow rate produces smaller droplets.
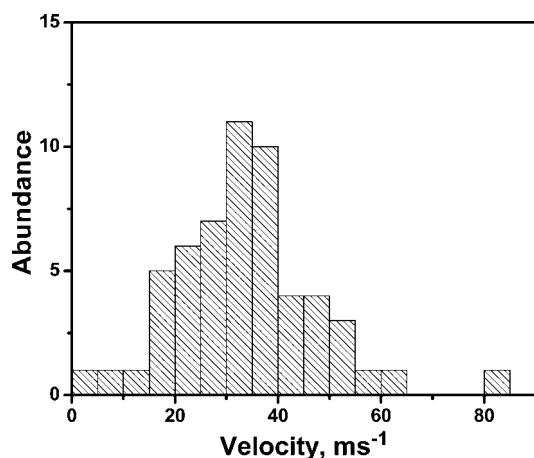
Figure 9. Histogram of the droplet velocities determined from the sonic spray photographs (Figure 7).

In Figure 7b the three overlaid images show the trajectories of the droplets. In the example shown here several of the droplets move in the focal plane of the camera, and so they are in focus in all three images. The time between the triggering of the different colored LEDs is known (10 μs), and so their positions can be used to determine their velocity. The distribution of velocities obtained from this analysis is shown in Figure 9. The distribution peaks at around 35 ms^{-1}. This is significantly smaller than for the droplets after they travel through the capillary interface (around 200−300 ms^{-1}). The speed of the sonic spray droplets depends on the gas flow and on their position in the gas stream.

Figure 10 shows a photograph of the droplets generated by the VOAG source. This image was recorded with 5× magnification at f/2.8. Under these conditions the depth of field is only around 40 μm. The image shows a stream of droplets emitted from the source. In this particular image there is a fairly wide distribution of droplet sizes. In many other images the distribution was narrower, but the size of the droplets varied

from image to image. It appears that we did not achieve a stable operating mode. Figure 8b shows a histogram of the droplet sizes deduced from the images. The distribution is broad, extending up to a radius of 120 μm, and peaks at around 40−60 μm. The average size of the droplets generated by VOAG (57 μm) is much larger than generated by sonic spray (26 μm).

Discussion

Measuring *m/z*: Pulsed Acceleration versus the Time Shift Approach. As described above, in previous work we used a pulsed acceleration approach to determine the masses of individual electrosprayed water droplets. This approach was tried for the sonic spray droplets but we found that the shift in the velocity was too small to determine the *m/z* ratio of individual droplets—the droplets from sonic spray evidently have a larger *m/z* ratio than those from electrospray. So we developed an alternative method, the time shift approach, which we believed would allow us to measure larger *m/z* ratios. However, we were still unable to measure the *m/z* ratios of individual sonic spray droplets with this approach, although an average value was obtained, from which we were able to estimate an average droplet radius.

In order to compare the two methods we start by estimating the largest *m/z* ratio that can be measured for an individual object by both methods. With the pulsed acceleration approach the *m/z* ratio is given by[28]

$$m/z = \frac{2eV_P}{m_u(v_f^2 - v_i^2)} \tag{4}$$

where V_P is the amplitude of the pulse and v_i and v_f are the velocities before and after pulsed acceleration, respectively. The largest *m/z* ratio that can be accurately measured is determined by the uncertainty in the velocity measurements, which can be obtained from the mean absolute difference in the velocities measured with the pulse acceleration turned off.[28] Using the value of 0.61 m/s from ref 28, a typical value for v_i (300 ms^{-1}),
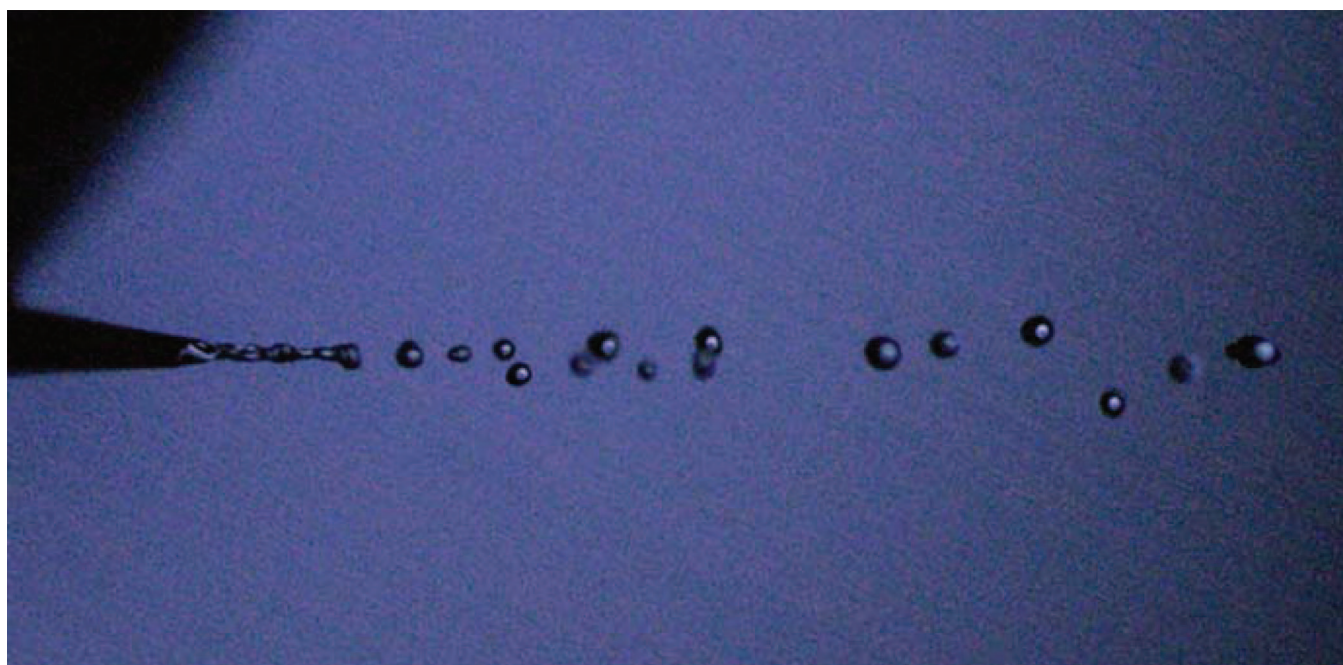

Figure 10. Photographs of the droplets generated by VOAG. The image was obtained by triggering a single white LED for 500 ns. The image was recorded while the source was attached to the image charge detection mass spectrometer.

Charge Separation in the Breakup of Water Droplets

J. Phys. Chem. A, Vol. 112, No. 51, 2008 **13359**

and $V_P = 3500$ V, the largest m/z ratio that can be determined is 1.84×10^9 Da.

With the time shift approach, the m/z ratio is given by eq 3. The largest m/z ratio that can be accurately measured is determined by the uncertainty in the time shift. The mean absolute time shift with the voltage to the time shift region turned off is 2.73 μs. Using this value along with $u = 300$ ms^{-1}, and $V = -20$ kV, eq 3 leads to 2.28×10^9 Da for the largest m/z ratio can be accurately measured for an individual object by the time shift approach. This value is only slightly larger than the value determined from the pulsed acceleration approach. In both cases, the accuracy of the m/z determination is limited by the accuracy of the measurement of the transit times through the image charge detectors. Raising the potential in the pulsed accelerator or in the time shift region will increase the accuracy of the m/z measurement and increase the largest mass that can be measured. An increase in the potential can more easily be accomplished for the time shift approach than for the pulsed acceleration. However, it is evident that there is not much difference between the performance of the two methods.

Droplet Sizes. The size of the droplets detected with the image charge detection mass spectrometer is similar for electrospray, sonic spray, and VOAG. In all cases the average droplet radius is around 2−3 μm. For positive mode electrospray we were able to measure the droplet size distribution, and the results have been reported elsewhere.[28] In this work, we attempted to measure the size distribution for sonic spray and VOAG droplets. However, the m/z ratios were too large to determine the distribution and we could only obtain the average radius. The main difference between the electrospray droplets and the sonic spray and VOAG droplets is that the former are more highly charged and, hence, have a lower m/z for a given radius.

The droplet sizes determined from the photographs of sonic spray and VOAG are both substantially larger than those detected by image charge detection mass spectrometry. The average radius obtained from the VOAG images is also substantially larger than the average radius from the sonic spray images, yet the average radii of the droplets determined by image charge detection mass spectrometry are similar for sonic spray and VOAG and much smaller. Both of these results point to the idea that the droplets are reduced in size or broken up somewhere in the apparatus prior to the detection region and most likely in the capillary interface.

Droplet Charges. There are several interesting features concerning the charge on the droplets. First, there is a clear preference for positively charged droplets in the image charge detection mass spectrometry measurements. The droplets detected from positive mode electrospray are predominantly (>99%) positively charged, as expected, but for negative mode electrospray only a minority (<30%) are negatively charged and most of the detected droplets (>70%) are positively charged.

With the electrospray voltage used here a corona discharge could occur at the end of the electrospray emitter,[38] and this might be the source of the oppositely charged droplets. However, we use a nonconducting electrospray emitter to inhibit corona discharge. On close inspection, we could not see any sign of the reddish or violet appearance usually associated with a corona discharge in air and we could not detect any ozone. Although some intermittent sparking occurred in negative mode electrospray, the electrospray current was always negative. It is difficult to imagine that positively charged droplets could be generated and travel to the capillary entrance under the conditions of

negative mode electrospray. In other words, the electrospray emitter is probably not the source of the positively charged droplets.

To test this idea further, we placed a series of three electrodes between the electrospray emitter and the capillary interface and biased the electrodes to transmit only regularly charged droplets and then only oppositely charged droplets. When biased to transmit only regularly charged droplets, we detected both regularly and oppositely charged droplets, and when biased to transmit only oppositely charged droplets we detected no droplets. These results support the notion that the oppositely charged droplets are formed downstream from the electrospray source. Finally, we note that the bias toward positively charged droplets is not limited to electrospray. The droplets from sonic spray and VOAG are also predominantly positively charged.

As the sonic spray source is electrically isolated the number of positive and negative charges leaving must balance. So we might expect the droplets to be randomly charged, and indeed random charging has been assumed for sonic spray.[39] Consider a droplet plucked from a solution containing anions and cations. If the droplet contains n ions, and each one can be either positive or negative, then the probability of the droplet having an overall charge z is given by

$$\Pi(z; n, p) = \frac{n!}{z!\,(n-z)!} p^Z (1-p)^Z \qquad (5)$$

where p is the probability of a particular charge state ($p = 0.5$ for + and −). For large n, the binomial distribution of eq 5 approaches a normal distribution

$$\Pi(z; z_0, \sigma) = \frac{1}{\sigma\sqrt{2\pi}} \exp\left(-\frac{(z - z_0)^2}{2\sigma^2}\right) \qquad (6)$$

where z_0 is the mean and σ is the standard deviation:

$$\sigma = \sqrt{np(1-p)} = \sqrt{n/4} \qquad (7)$$

For random charging, the mean is zero. However, the sonic spray droplets detected by image charge detection mass spectrometry are predominantly positively charged. This is not due to an electric field. No voltage is applied to the sonic spray source. The sonic spray droplets are less highly charged than the electrospray droplets, which is expected.

We now compare the charge on the sonic spray droplets with what is expected for random charging. The number of OH$^-$ and H$^+$ ions in pure water at room temperature is 2×10^{-7} mol/L or 1.20×10^{17} ions/L. A droplet with a radius of 2.7 μm has a volume of 8.24×10^{-14} L, and so it contains on average around 10 000 OH$^-$ and H$^+$ ions. The average deviation from the mean is

$$\bar{z} = \frac{\int_0^\infty z \exp(-2z^2/n)\,\mathrm{d}z}{\int_0^\infty \exp(-2z^2/n)\,\mathrm{d}z} = \left(\frac{n}{2\pi}\right)^{1/2} \qquad (8)$$

For $n = 10\,000$, $\bar{z} = 40$. As noted above, the average charge determined for the sonic spray droplets by image charge detection mass spectrometry is around 12 000 e. Clearly the charge on the sonic sprayed droplets (and the VOAG droplets, which have a similar average radius and average charge) is several orders of magnitude larger than expected from random charging.

Droplet Evaporation. The average radii of the droplets determined from the photographs (i.e., before passage through the capillary interface) is 26 μm for sonic spray and 57 μm for VOAG. The $\bar{z}$ values for these radii are 1185 and 3850,

respectively. Let us now consider the possibility that the large droplets generated by sonic spray and VOAG evaporate down to the smaller droplets observed by image charge detection mass spectrometry, while retaining their charge (which remains well below the Rayleigh limit). The $\bar{z}$ values are still too small to account for the charges observed on the sonic spray and VOAG droplets, but they are the same order of magnitude, and so we consider this possibility further.

The VOAG and sonic spray sources are both around 1 cm from the entrance of the capillary. The average velocity of the sonic spray droplets is 34 ms^{-1} (from Figure 9), so the average transit time is 0.3 ms. The average velocity of the VOAG droplets was not measured, but it is expected to be less than the sonic spray droplets. We estimate the transit time through the capillary using the Poiseuille equation[40]

$$\Delta P = \frac{8 \eta L Q}{\pi r^4} \tag{9}$$

which gives the pressure difference, ΔP, required for the flow of an incompressible fluid through a circular pipe. η in eq 9 is the dynamic viscosity, L is the length, and Q is the volume flow. We divide the capillary into small lengths and apply the Poiseuille equation to each section sequentially, adjusting the pressure and volume flow using the ideal gas equation. The volume flow at the entrance of the capillary was estimated from the pressure and effective pumping speed in the first differentially pumped region. With the use of this approach, the transit time through the capillary is estimated to be around 0.5 ms. So the total transit time (from the source to the capillary exit) is ~1 ms for sonic spray.

The mass rate of change of a water droplet in air is[1]

$$\frac{dm}{dt} = \frac{4\pi r D_V^* M}{R} \left(\frac{p_\infty}{T_\infty} - \frac{p_{sat}}{T_a} \right) \tag{10}$$

where M is the molar mass of water, R is the gas constant, p_∞ is the ambient water vapor partial pressure, p_{sat} is the equilibrium vapor pressure, T_∞ is the ambient temperature, T_a is the droplet temperature, and D_V^* is the effective gas-phase diffusion coefficient of water in air, given by

$$D_V^* = \frac{D_V}{\dfrac{r}{r+\lambda} + \dfrac{4 D_V}{r \alpha \bar{v}_w}} \tag{11}$$

where λ is the mean free path of a water molecule in air, $\bar{v}_w$ is the mean molecular speed of a gas-phase water molecule, and α is the mass accommodation coefficient. Figure 11 shows the time scale for evaporating water droplets with initial radii of 2, 5, 10, 20, and 40 μm with $T_a = T_\infty = 293$ K and 50% relative humidity. This approach ignores the evaporative cooling of the droplet, which will decrease the evaporation rate, and also ignores that fact that the droplet is not stationary, which may increase the evaporation rate. However, the evaporation times for 20 and 40 μm droplets are orders of magnitude larger than the transit time to and through the capillary (<10^{-3} s). Also, as is evident from Figure 11, once the droplet's radius starts decreasing rapidly, the droplet quickly disappears. It is difficult to imagine that evaporation of larger droplets from different sources (electrospray, sonic spray, and VOAG) should all stop at droplets with radii around 2−3 μm. Once the droplets enter the vacuum chamber, rapid evaporative cooling will supercool the droplets, and they may subsequently freeze.[41] During evaporative cooling, the droplet radii will shrink by about 5%.[42] Thus, evaporation is not the primary reason why the droplets
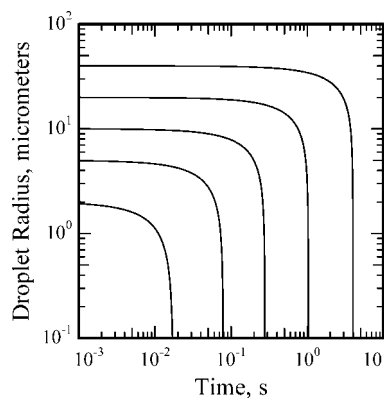

Figure 11. Plot of droplet radius against time showing the effect of evaporation for initial droplet radii of 2, 5, 10, 20, and 40 μm. The simulations were performed at room temperature for a relative humidity of 50%. See text for a description of the model used for the simulation.

detected by image charge detection mass spectrometry are much smaller than the droplets initially generated by sonic spray and VOAG.

Aerodynamic Breakup in the Capillary Interface. When the droplets enter the capillary interface the gas flow velocity is much faster than the velocity of the droplet. This leads to an aerodynamic force on the droplet which causes it to accelerate. The aerodynamic force can also cause the droplet to break up. The breakup of liquid droplets in a gas stream is a well-studied process. Experiments show that droplets suddenly placed in a high-speed flow will break up if the Weber number exceeds ~10.[43,44] The Weber number is given by

$$We = \frac{\rho_G v^2 d}{\sigma} \tag{12}$$

where ρ_G is the gas density, v is the velocity of the gas flow relative to the droplet, d is the diameter of the droplet, and σ is the surface tension. For a water droplet with a radius of 57 μm (the average from the VOAG), $We = 10$ when $v = 73$ ms^{-1}. The average flow velocity at the entrance of the capillary is around 170 ms^{-1}, well above that required to break up a 57 μm droplet. The maximum flow velocity is a factor of 2 larger than the average (340 ms^{-1}) if the flow is laminar. Even higher flow velocities are expected at the exit of the capillary where the flow velocity is expected to approach the terminal flow velocity for a perfect isentropic expansion of air at 300 K (780 ms^{-1}).[45] Although the gas density is lower at the exit of the capillary, the much larger gas velocity can compensate so that conditions are right at both the entrance and exit of the capillary for the droplets to be aerodynamically broken up.

As can be seen from eq 12, the velocity differential required for breakup increases as the droplet size decreases. Furthermore, as the droplet size decreases they are more easily accelerated, reducing the flow differential. So aerodynamic breakup in the capillary should reduce the droplets to a common size, which is relatively independent of the initial size. This is consistent with the results we have obtained from sonic spray and VOAG, where the droplets have substantially different average sizes on the atmosphere side of the capillary interface (average radii of 26 and 57 μm, respectively) but similar, and much smaller, sizes according to image charge detection mass spectrometry. From eq 12 we can get an estimate of the largest droplets that should be transmitted through the capillary interface. Using the average flow velocity at the entrance of the capillary (170 ms^{-1}), the maximum radius that is stable is ~10 μm, and for the maximum
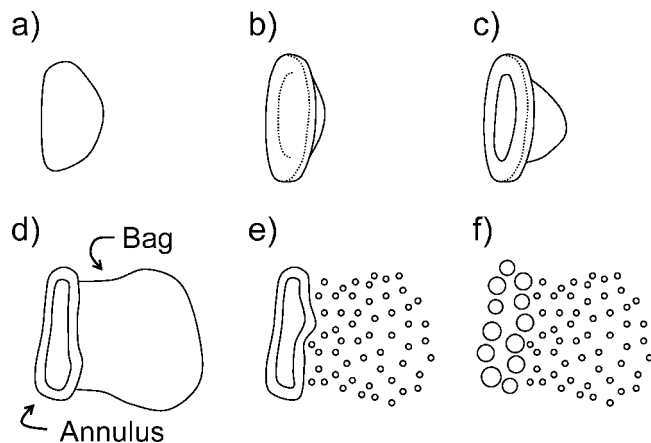
Charge Separation in the Breakup of Water Droplets

J. Phys. Chem. A, Vol. 112, No. 51, 2008 **13361**

Figure 12. Cartoon illustrating the bag mechanism for the aerodynamic breakup of a droplet.

Figure 13. Cartoon showing how charge separation may occur during aerodynamic breakup by the bag mechanism.

flow velocity (340 ms^{-1}) it is ∼2.5 μm. This is consistent with our experimental observations where the average radii of the droplets from VOAG and sonic spray are both ∼3 μm.

We have not yet considered how the droplets break up. Krzeczkowski has identified several kinds of droplet breakup processes that occur over different ranges of Weber numbers.[43] At low Weber numbers breakup occurs mainly through the bag breakup mechanism[46−48] shown schematically in Figure 12. Here, the droplet first flattens (a), a dimple forms (b), and then a bag or bubble, supported by an annulus, is blown out from the center (c and d). The bag bursts generating many small droplets (e), and then the annulus breaks up into a few large droplets (f).

Charge Separation During Aerodynamic Breakup. The aerodynamic breakup of the droplets in the capillary interface can account for the size of the droplets detected by image charge detection mass spectrometry and the fact that the size is independent of the initial size of the droplets as they enter the capillary. Can the same process account for the charging phenomena observed here: (1) the higher than expected charge found on droplets from VOAG and sonic spray, (2) the preference for positive charge on droplets from sonic spray, VOAG, and electrospray, and (3) the formation of oppositely charged droplets from electrospray?

It has been known for many years that the aerodynamic breakup of water droplets in air leads to charge separation.[12,13] The charge separation associated with splashing and bubbling of water has also been studied for many years.[11,49] This phenomena has been attributed to the presence of an electrical double layer at the surface of water, where the outermost layers acquire an excess negative charge. There is strong and compelling support for this view from electrophoretic mobility measurements for air bubbles in water, which show that they move as if they have an excess negative charge.[50,51]

The question of the molecular origin of the excess negative charge is not yet fully resolved. It probably follows from oriented dipoles at the water−vapor interface, a suggestion clearly laid out 80 years ago.[52] Vibrational sum frequency generation spectroscopic measurements at the interfacial region of water have shown that 20−30% of molecules exhibit dangling hydrogens.[53] This leaves 70−80% of interfacial water dipoles with their positive end directed toward the water interior. Paluch has reviewed theoretical calculations that support this general view.[54] This picture is also confirmed by surface potential measurements. The accepted value for the surface potential of water is +0.10 V.[55] A positive value indicates that the water
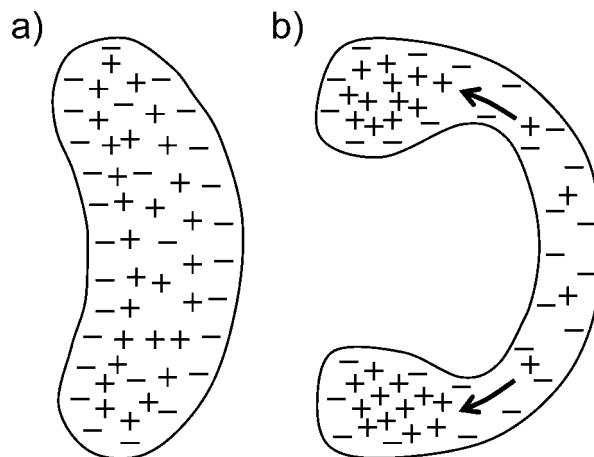
dipoles are preferentially oriented with the negative pole toward the gas phase.

Although the electric field of a surface layer of dipoles drops off to negligible values beyond a few molecular diameters,[56] its value at short range is considerable. In particular, the attraction of small ions close to the water dipole can approach 100 kJ/mol.[56] Thus, some of the OH$^-$ ions in the bulk are electrostatically drawn to the oriented water dipoles at the surface, leaving the interfacial region negatively charged. The concentration of the charge balancing H$_3$O$^+$ ions falls off exponentially from the interface on a scale of around 1 μm—the Debye distance for pure water.[56]

Studies of the charge separation in the aerodynamic breakup of water droplets have shown that the positive charge is carried by large fragments and the negative charge is carried by much smaller fragments. Figure 13 illustrates how such charge separation could occur. Excess OH$^-$ ions are attracted to the interfacial region by the positive end of the surface dipoles. As the bag forms and thins, the H$_3$O$^+$ counterions are swept into the annulus. When the bag breaks it generates a large number of small negatively charged fragments, and when the annulus breaks it produces a small number of large positively charged fragments. The positively charged droplets are detected, but the charge on the negatively charged fragments is below the detection limit of the charge detectors (∼1000−2000 e).

To illustrate the breakup, consider a droplet with a 10 μm radius. We can reasonably assume that half of the volume goes into the bag and half goes into the annulus. Then the bag can blow up to ∼80 μm radius before the wall thickness reaches 25 nm (a reasonable minimum). At this point the surface area of the bubble is 64 times larger than the surface area of the original droplet, and so electrostatic repulsion between charges on the surface of the bubble is dramatically reduced. If we assume that the annulus breaks up into 10 droplets, the volume of the large droplet fragments will be around $^1/_{20}$ of the volume of the initial droplet corresponding to a radius of 3.7 μm. Thus, the breakup can be expected to reduce the radius by around a factor of 3. Droplets generated by sonic spray (average radius ∼26 μm) and by VOAG (average radius ∼57 μm) will thus undergo several sequential breakups before reaching the terminal size of ∼3 μm detected by image charge detection mass spectrometry.

Although there have been several studies of the charge separation in the breakup of uncharged droplets, dating back to 1909, we are unaware of any studies of the aerodynamic breakup

of charged droplets. The excess negative charge on a negatively charged droplet will tend to localize on the bag surface during breakup. And so the negative charge will be distributed over many small droplets and will not be detected in our experiments because a charge of at least 10^3 e is required. This explains why we see far fewer droplets from negative mode electrospray than from positive mode. The excess positive charge on a positively charged droplet will tend to localize on the annulus rather than on the surface area of the bag. And so when the droplet breaks up the positive charge will go to the larger fragments from the annulus. The surface areas of the bag and the annulus are both larger than the surface area of a spherical droplet, so dispersion of the excess charge on the bag and the annulus is favored from an electrostatic point of view, though obviously the bag, with a larger surface area, is more favorable.

Charge separation during the breakup of a charged droplet can also account for the oppositely charged droplets found in electrospray. This is most easily seen by considering a negatively charged droplet. As described above, when an uncharged droplet breaks up, the bag is expected to attain a negative charge and the annulus a positive charge. If the droplet is slightly negatively charged then the excess negative charge will go to the bag, but there can still be charge separation with the bag acquiring the extra negative charge and the annulus the corresponding positive charge. If the initial charge on the droplet is increased, eventually it will become large enough to inhibit further charge separation.

Conclusions

Digital macrophotography and image charge detection mass spectrometry have been used to study charged water droplets generated by electrospray, sonic spray, and VOAG. Our three main experimental observations are the following:

1 The droplets transmitted through the capillary interface and detected by image charge detection mass spectrometry are reduced to approximately the same radius (2−3 μm) regardless of the initial size of the droplet.

2 The average charge on the droplets generated by VOAG and sonic spray is much larger than expected for random charging.

3 Positively charged droplets are much more prevalent than negatively charged ones.

These observations can all be accounted for by the aerodynamic breakup of the droplets as they are accelerated in the capillary interface. As the droplets become smaller, larger relative air velocities are required to break them up, and so with fixed capillary flow conditions they reach a terminal size that is relatively independent of their initial size. With the capillary flow conditions employed here the critical Weber number is consistent with a terminal size of around 3 μm. The relatively high charge on the droplets from sonic spray and VOAG result from charge separation during the breakup of the droplets. The charge separation and the preference for positively charged droplets results from the bag mechanism by which the droplets break up and the fact that there is an electrical bilayer at the surface of water with the interfacial layer having a slight excess of OH^-.

Although the aerodynamic breakup of the droplets appears to account for the experimental observations, there is no direct evidence that this process occurs, and so we do not completely rule out other explanations for our observations. The bipolar fission suggested previously[27] could still account for the detection of a small fraction (<1%) of negatively charged droplets from positive mode electrospray. Other factors may also play a role, like charge separation during freezing and fracture of droplets that are evaporatively cooled in vacuum. We will address this issue in a future publication.

In electrospray mass spectrometry pure water is rarely used as the solvent. Usually a mixture of solvents is employed, such as water and methanol, and the solution is acidified. We do not know to what extent the results reported here for pure water droplets will transfer to the solutions used in electrospray mass spectrometry. The aerodynamic breakup of the droplets will still take place, and it will occur for smaller droplets if the surface tension is reduced. However, we do not know how much charge separation occurs in the breakup of droplets of the solvent mixtures usually used in electrospray mass spectrometry.

References and Notes

(1) Pruppacher, H. R.; Klett, J. D. *Microphysics of Clouds and Precipitation*, 2nd ed.; Kluwer Academic Publishers: Dordrecht, The Netherlands, 1997.

(2) MacGorman, D. R.; Rust, W. D. *The Electrical Nature of Storms*; Oxford University Press: New York, 1998.

(3) Reynolds, S. E.; Brook, M.; Gourley, M. Thunderstorm Charge Separation. *J. Meteorol.* **1957**, *14*, 426–436.

(4) Takahashi, T. Riming Electrification as a Charge Generation Mechanism in Thunderstorms. *J. Atmos. Sci.* **1978**, *35*, 1536–1548.

(5) Brooks, I. M.; Saunders, C. P. R. An Experimental Investigation of the Inductive Mechanism of Thunderstorm Electrification. *J. Geophys. Res., [Atmos.]* **1994**, *99*, 10627–10632.

(6) Mason, J.; Mason, N. The Physics of a Thunderstorm. *Eur. J. Phys.* **2003**, *24*, S99–S110.

(7) Avila, E. E.; Saunders, C. P. R.; Bax-Norman, H.; Castellano, N. E. Charge Sign Reversal in Irregular Ice Particle−Graupel Collisions. *Geophys. Res. Lett.* **2005**, *32*, L01801.

(8) Mansell, E. R.; MacGorman, D. R.; Ziegler, C. L.; Straka, J. M. Charge Structure and Lightning Sensitivity in a Simulated Multicell Thunderstorm. *J. Geophys. Res., [Atmos.]* **2005**, *110*, D12101.

(9) Bürgesser, R. E.; Pereyra, R. G.; Avila, E. E. Charge Separation in Updraft of Convective Regions of Thunderstorm. *Geophys. Res. Lett.* **2006**, *33*, L03808.

(10) Sherwood, S. C.; Phillips, V. T. J.; Wettlaufer, J. S. Small Ice Crystals and the Climatology of Lightning. *Geophys. Res. Lett.* **2006**, *33*, L05804.

(11) Lenard, P. Ueber die Electricät der Wasserfälle. *Ann. Phys.* **1892**, *46*, 584–636.

(12) Simpson, G. C. On the Electricity of Rain and its Origin in Thunderstorms. *Philos. Trans. R. Soc. London* **1909**, *A209*, 379–413.

(13) Zeleny, J. Variation with Temperature of the Electrification Produced in Air by the Disruption of Water Drops and its Bearing on the Prevalence of Lightning. *Phys. Rev.* **1933**, *44*, 837–842.

(14) Yamashita, M.; Fenn, J. B. Electrospray Ion Source. Another Variation on the Free Jet Theme. *J. Phys. Chem.* **1984**, *88*, 4451–4459.

(15) Fenn, J. B.; Mann, M.; Meng, C. K.; Wong, M. G.; Whitehouse, C. M. Electrospray Ionization for Mass Spectrometry of Large Biomolecules. *Science* **1989**, *246*, 64–71.

(16) Cole, R. B. Some Tenets Pertaining to Electrospray Ionization Mass Spectrometry. *J. Mass Spectrom.* **2000**, *35*, 763–772.

(17) Gamero-Castaño, M.; Fernandez de la Mora, J. Kinetics of Small Ion Evaporation from the Charge and Mass Distribution of Multiply Charged Clusters in Electrosprays. *J. Mass Spectrom.* **2000**, *35*, 790–803.

(18) Kebarle, P. A Brief Overview of the Present Status of the Mechanisms Involved in Electrospray Mass Spectrometry. *J. Mass Spectrom.* **2000**, *35*, 804–817.

(19) Kebarle, P.; Peschke, M. On the Mechanism by which the Charged Droplets Produced by Electrospray Lead to Gas Phase Ions. *Anal. Chim. Acta* **2000**, *406*, 11–35.

(20) Cech, N. B.; Enke, C. G. Practical Implications of Some Recent Studies in Electrospray Ionization Fundamentals. *Mass Spectrom. Rev.* **2001**, *20*, 362–387.

(21) Lord Rayleigh. On the Equilibrium of Liquid Conducting Masses Charged with Electricity. *Philos. Mag.* **1882**, *14*, 184−186.

(22) Dole, M.; Mack, L. L.; Hines, R. L.; Mobley, R. C.; Ferguson, L. D.; Alice, M. B. Molecular Beams of Macroions. *J. Chem. Phys.* **1968**, *49*, 2240–2249.

(23) Mack, L. L.; Kralik, P.; Rheude, A.; Dole, M. Molecular Beams of Macroions. II. *J. Chem. Phys.* **1970**, *52*, 4977–4986.

Charge Separation in the Breakup of Water Droplets

J. Phys. Chem. A, Vol. 112, No. 51, 2008 **13363**

(24) Iribarne, J. V.; Thomson, B. A. On the Evaporation of Small Ions from Charged Droplets. *J. Chem. Phys.* **1976**, *64*, 2287–2294.

(25) Hirabayashi, A.; Sakairi, M.; Koizumi, H. Sonic Spray Ionization Method for Atmospheric Pressure Ionization Mass Spectrometry. *Anal. Chem.* **1994**, *66*, 4557–4559.

(26) Hirabayashi, A.; Sakairi, M.; Koizumi, H. Sonic Spray Mass Spectrometry. *Anal. Chem.* **1995**, *67*, 2878–2882.

(27) Maze, J. L.; Jones, T. C.; Jarrold, M. F. Negative Droplets from Positive Electrospray. *J. Phys. Chem. A* **2006**, *110*, 12607–12612.

(28) Mabbett, S. R.; Zilch, L. W.; Maze, J. T.; Smith, J. W.; Jarrold, M. F. Pulsed Acceleration Charge Detection Mass Spectrometry: Application to Weighing Electrosprayed Droplets. *Anal. Chem.* **2007**, *79*, 8431–8439.

(29) Sanford, F. Negatively Electrified Rain Droplets. *Phys. Rev.* **1918**, *11*, 445–448.

(30) Takats, Z.; Nanita, S. C.; Cooks, R. G.; Schlosser, G.; Vekey, K. Amino Acid Clusters Formed by Sonic Spray Ionization. *Anal. Chem.* **2003**, *75*, 1514–1523.

(31) Fuerstenau, S. D.; Benner, W. H. Molecular Weight Determination of Megadalton DNA Electrospray Ions Using Charge Detection Time-of-Flight Mass Spectrometry. *Rapid Commun. Mass Spectrom.* **1995**, *9*, 1528–1538.

(32) Zeleny, J. Instability of Electrified Liquid Surfaces. *Phys. Rev.* **1917**, *10*, 1–6.

(33) Taylor, G. Disintegration of Water Drops in an Electric Field. *Proc. R. Soc. London, Ser. A* **1964**, *280*, 383–397.

(34) The effective length of the detector is determined from measurements made without a voltage on the acceleration region. The effective length is determined from the transit time through the detectors, the transit time between the detectors, and the known distance between the detectors.

(35) Juraschek, R.; Röllgen, F. W. Pulsation Phenomena during Electrospray Ionization. *Int. J. Mass Spectrom.* **1998**, *177*, 1–15.

(36) From $\sigma_S = (\sigma_{V+S}{}^2 - \sigma_V{}^2)^{1/2}$, where σ_{V+S} is the standard deviation determined for the shifted distribution (which includes contributions from both the uncertainty in the velocity determination and the variation in the time shifts), σ_V is the standard deviation for the unshifted distribution (which results only from the uncertainty in the velocity measurements), and σ_S is the standard deviation due to the variation in the time shift.

(37) SIMION is a software package primarily used to calculate electric fields and the trajectories of charged particles in those fields. See: http://www.simion.com/.

(38) Ikonomou, M. G.; Blades, A. T.; Kebarle, P. Electrospray Mass Spectrometry of Methanol and Water Solutions Suppression of Electric Discharge with SF_6 Gas. *J. Am. Soc. Mass Spectrom.* **1991**, *2*, 497–505.

(39) Van Berkel, G. J. An Overview of Some Recent Developments in Ionization Methods for Mass Spectrometry. *Eur. J. Mass Spectrom.* **2003**, *9*, 539–562.

(40) Tison, S. A. Experimental Data and Theoretical Modeling of Gas Flows through Metal Capillary Leaks. *Vacuum* **1993**, *44*, 1171–1175.

(41) Huang, J.; Bartell, L. S. Kinetics of Homogeneous Nucleation in the Freezing of Large Water Clusters. *J. Phys. Chem.* **1995**, *99*, 3924–3931.

(42) Based on a rough estimate for cooling from 293 to 200 K using the bulk heat capacity of water and the bulk latent heat of evaporation.

(43) Krzeczkowski, S. A. Measurement of Liquid Droplet Disintegration Mechanisims. *Int. J. Multiphase Flow* **1980**, *6*, 227–239.

(44) Wierzba, A. Deformation and Breakup of Liquid Drops in a Gas Stream at Nearly Critical Weber Numbers. *Exp. Fluids* **1990**, *9*, 59–64.

(45) See, for example: (a) Silbey, R. J.; Alberty, R. A.; Bawendi, M. G. *Physical Chemistry*, 4th ed.; Wiley: New York, 2005; p 703. (b) De Paul, S.; Pullman, D.; Friedrich, B. A. Pocket Model of a Seeded Supersonic Expansion. *J. Phys. Chem.* **1993**, *97*, 2167–2171.

(46) Hochschwender, E. Dissertation, Heidelberg University, 1919.

(47) Lane, W. H. Shatter of Drops in Streams of Air. *Ind. Eng. Chem.* **1951**, *43*, 1312–1317.

(48) Matthews, J. B.; Mason, B. J. Electrification Produced by the Rupture of Large Water Drops in an Electric Field. *Q. J. R. Meteorol. Soc.* **1964**, *90*, 275–286.

(49) Blanchard, D. C. *From Raindrops to Volcanoes: Adventures with Sea Surface Meteorology*; Dover: Mineola, NY, 2004.

(50) Takahashi, M. ζ-Potential of Microbubbles in Aqueous Solutions: Electrical Properties of the Gas−Water Interface. *J. Phys. Chem. B* **2005**, *109*, 21858–21864.

(51) Creux, P.; Lachaise, J.; Graciaa, A.; Beattie, J. K. Specific Cation Effects at the Hydroxide−Charged Air/Water Interface. *J. Phys. Chem. C* **2007**, *111*, 3753–3755.

(52) Currie, B. W.; Alty, T. Absorption at a Water Surface. Part 1. *Proc. R. Soc. London* **1929**, *122*, 622–633.

(53) Miranda, P. B.; Shen, Y. R. Liquid Interfaces: A Study by Sum-Frequency Vibrational Spectroscopy. *J. Phys. Chem. B* **1999**, *103*, 3292–3307.

(54) Paluch, M. Electrical Properties of Free Surface of Water and Aqueous Solutions. *Adv. Colloid Interface Sci.* **2000**, *84*, 27–45.

(55) Parfenyuk, V. I. Surface Potential at the Gas−Aqueous Solution Interface. *Colloid J.* **2002**, *64*, 588–595.

(56) Israelachvili, J. N. *Intermolecular and Surface Forces (With Applications to Colloidal and Biological Systems)*, 2nd ed.; Elsevier, 1991.